Preprints (www.preprints.org) | NOT PEER-REVIEWED | Posted: 5 August 2022 doi:10.20944/preprints202208.0126.v1

GRAPHICAL ABSTRACT

Encapsulation Studies and *In Silico* Identification of Protein Targets Associated to the Insecticide Activity of Eugenol Derivatives

Maria José G. Fernandes[1±], Renato B. Pereira[2±], Ana Rita O. Rodrigues[3,4], Tatiana F. Vieira[5,6], A. Gil Fortes[1], David M. Pereira[2], Sérgio F. Sousa[5,6], Elisabete M. S. Castanheira[3,4], M. Sameiro T. Gonçalves[1*]

* msameiro@quimica.uminho.pt

[1] Centre of Chemistry, Department of Chemistry, University of Minho, *Campus* of Gualtar, 4710-057 Braga, Portugal.

[2] REQUIMTE/LAQV, Laboratory of Pharmacognosy, Department of Chemistry, Faculty of Pharmacy, University of Porto, R. Jorge Viterbo Ferreira, 228, 4050-313 Porto, Portugal.

[3] Physics Centre of Minho and Porto Universities (CF-UM-UP), University of Minho, *Campus* of Gualtar, 4710-057 Braga, Portugal.

[4] Associate Laboratory LaPMET - Laboratory of Physics for Materials and Emergent Technologies, University of Minho, *Campus* of Gualtar, 4710-057 Braga, Portugal.

[5] UCIBIO/REQUIMTE, BioSIM – Department of Medicine, Faculty of Medicine, University of Porto, Alameda Prof. Hernâni Monteiro, 4200-319 Porto, Portugal.

[6] Associate Laboratory i4HB - Institute for Health and Bioeconomy, Faculty of Medicine, University of Porto, 4200-319 Porto, Portugal.

[±] These authors contributed equally to this work

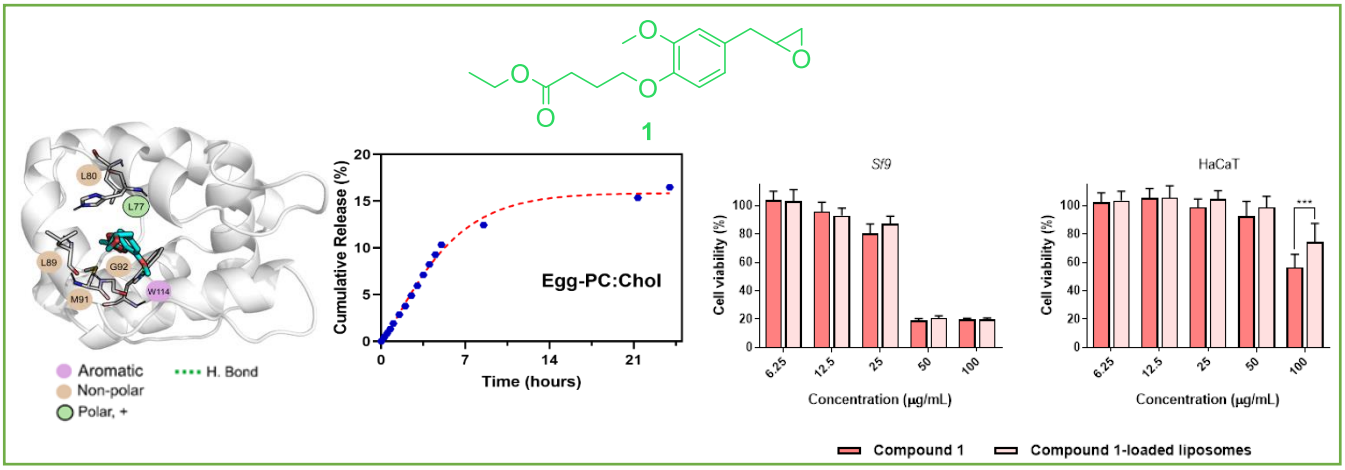

Preprints (www.preprints.org) | NOT PEER-REVIEWED | Posted: 5 August 2022 doi:10.20944/preprints202208.0126.v1

Encapsulation Studies and *In Silico* Identification of Protein Targets Associated to the Insecticide Activity of Eugenol Derivatives

Maria José G. Fernandes[1±], Renato B. Pereira[2±], Ana Rita O. Rodrigues[3,4], Tatiana F. Vieira[5,6], A. Gil Fortes[1], David M. Pereira[2], Sérgio F. Sousa[5,6], Elisabete M. S. Castanheira[3,4], M. Sameiro T. Gonçalves[1*]

* msameiro@quimica.uminho.pt

[1] Centre of Chemistry, Department of Chemistry, University of Minho, *Campus* of Gualtar, 4710-057 Braga, Portugal.

[2] REQUIMTE/LAQV, Laboratory of Pharmacognosy, Department of Chemistry, Faculty of Pharmacy, University of Porto, R. Jorge Viterbo Ferreira, 228, 4050-313 Porto, Portugal.

[3] Physics Centre of Minho and Porto Universities (CF-UM-UP), University of Minho, *Campus* of Gualtar, 4710-057 Braga, Portugal.

[4] Associate Laboratory LaPMET - Laboratory of Physics for Materials and Emergent Technologies, University of Minho, *Campus* of Gualtar, 4710-057 Braga, Portugal.

[5] UCIBIO/REQUIMTE, BioSIM – Department of Medicine, Faculty of Medicine, University of Porto, Alameda Prof. Hernâni Monteiro, 4200-319 Porto, Portugal.

[6] Associate Laboratory i4HB - Institute for Health and Bioeconomy, Faculty of Medicine, University of Porto, 4200-319 Porto, Portugal.

[±] These authors contributed equally to this work

Abstract

The eugenol derivative, ethyl 4-(2-methoxy-4-(oxiran-2-ylmethyl)phenoxy)butanoate **1**, with promising insecticidal capability was encapsulated in liposomal formulations of egg-phosphatidylcholine/cholesterol (Egg-PC:Ch) 70:30 and of 100% dioleoylphosphatidylglycerol (DOPG). Compound-loaded Egg-PC:Ch liposomes exhibit small hydrodynamic diameters (below 100 nm), high encapsulation efficiency (88.8% ± 2.7%), higher stability and a more efficient compound release, being chosen for assays in *Sf9* insect cells. Compound **1** elicited a loss of cell viability up to 80% after 72h of incubation. Relevantly, encapsulation maintained the toxicity of compound **1** towards insect cells, while it lowered toxicity towards human cells, thus showing the selectivity of the system.

Structure based inverted virtual screening was used to predict the most likely targets and molecular dynamics simulations and free energy calculations were used to demonstrate that this molecule can form a stable complex with insect odorant binding proteins and/or acetylcholinesterase.

 doi:10.20944/preprints202208.0126.v1

Keywords: Eugenol; Essential oils; Nanoencapsulation; Biopesticides; Insecticides; Odorant binding proteins; Inverted virtual screening

1. Introduction

The synthesis of new bioinspired insecticides is of huge relevance in agriculture, considering that these compounds can eradicate pests with high activity and low toxicity, being ecofriendly substituents of the synthetic insecticides [1]. Eugenol exhibits a potent insecticidal activity and the synthesis of new derivatives can be an important way to modulate the biological activity of these compounds [2]. A set of *O*-alkylated eugenol (trivial name for 4-allyl-2-methoxyphenol) derivatives, having a propyl chain with terminals such as hydrogen, hydroxyl, ester, chlorine and carboxylic acid, and their later epoxidation to give the corresponding oxiranes, was previously published by our research group [3]. All derivatives were evaluated against their effect upon the viability of insect cell line *Sf*9 (*Spodoptera frugiperda*), evidencing that structural changes elicit marked effects in terms of potency [3].

In continuation of the former study, this work presents the application of an integrated molecular modelling – inverted virtual screening protocol for the identification of potential protein targets for the eugenol derivatives previously reported. The protocol included the study of protein targets typically associated with the insecticide activity and five different scoring functions from popular docking software alternatives. *O*-Alkylated oxiranes bearing the propyl chain with ester and chloride as terminals turned out to be very promising for future applications as active ingredients in insecticide formulations, with equally important low toxicity towards human cells after 24 h treatment [3]. In order to understand whether the impacts these two eugenol oxiranes, namely ethyl 4-(2-methoxy-4-(oxiran-2-ylmethyl)phenoxy)butanoate **1** and 2-(4-(3-chloropropoxy)-3-methoxybenzyl)oxirane **2** were time-dependent, the cytotoxic effects to *Sf9* cells were evaluated after 72 h exposure. Additional *in silico* assays were performed to predict possible targets for these eugenol derivatives. Through an Inverted Virtual Screening approach, 23 common pesticide targets were screened and the top two targets predicted were further evaluated through molecular dynamics simulations and free energy calculations.

In order to circumvent some common limitations of nature-inspired pesticides, which difficult their application, such as reduced stability, volatility, low water solubility, poor bioavailability, and low resistance to the presence of oxygen and light, the eugenol oxirane, ethyl 4-(2-methoxy-4-(oxiran-2-ylmethyl)phenoxy)butanoate **1** was submitted to nanoencapsulation assays in a liposomal system. In fact, encapsulation techniques have arisen as suitable strategies for the preservation of biopesticides

Preprints (www.preprints.org) | NOT PEER-REVIEWED | Posted: 5 August 2022 doi:10.20944/preprints202208.0126.v1

[4,5] More specifically, lipid-based carriers have been widely used as vehicles for cosmetic/pharmaceutical bioactives, plant extracts and pesticides [6-10]. The results here obtained point out the potential application of these nanosystems in future eugenol-based insecticide formulations.

2. Results and discussion

*2.1.Toxicity of **1** and **2** towards insect cells have a time-dependent effect*

Ethyl 4-(2-methoxy-4-(oxiran-2-ylmethyl)phenoxy)butanoate **1** and 2-(4-(3-chloropropoxy)-3-methoxybenzyl)oxirane **2** (Fig. 1) were obtained by epoxidation with *m*-chloroperbenzoic acid in dichloromethane at room temperature of ethyl 4-(4-allyl-2-methoxyphenoxy)butanoate and 4-allyl-1-(3-chloropropoxy)-2-methoxybenzene, respectively, which resulted from *O*-alkylation of eugenol, trivial name for 4-allyl-2-methoxyphenol, with ethyl 4-bromobutanoate or 1-bromo-3-chloro-propane, using cesium carbonate in acetonitrile, at 65 ºC. The compounds presented a purity ≥ 95% according to the ^{1}H NMR spectra [3].

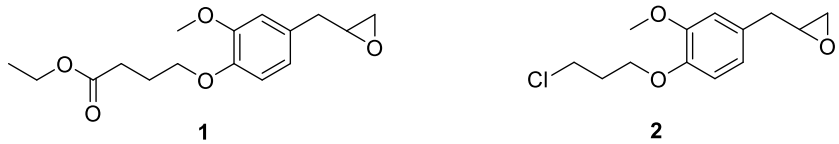

Fig. 1. Structure of ethyl 4-(2-methoxy-4-(oxiran-2-ylmethyl)phenoxy)butanoate **1** and 2-(4-(3-chloropropoxy)-3-methoxybenzyl)oxirane **2**.

Continuing our ongoing research on the insecticidal properties of eugenol-based molecules [3,11], we were particularly interested in exploring whether the impacts of oxiranes **1** and **2** on *Sf9* cell viability were time-dependent. With this aim in view, *Sf9* cells were treated during 72h with both molecules at five different concentrations (6.25 – 100 µg/mL) and compared with the results previously reported after 24h exposure [3]. As shown in Fig. 2, compounds **1** and **2**, after 72 h treatment, caused *ca* 80% loss of viability at 100 µg/mL, a result markedly different that what have been found at 24 h [3]. Furthermore, compound **1** displayed the capacity to trigger a similar effect even at 50 µg/mL, being clearly more toxic to *Sf9* cells than compound **2**. For this reason, oxirane **1** was chosen for further computational and nanoencapsulation studies.

Preprints (www.preprints.org) | NOT PEER-REVIEWED | Posted: 5 August 2022 doi:10.20944/preprints202208.0126.v1

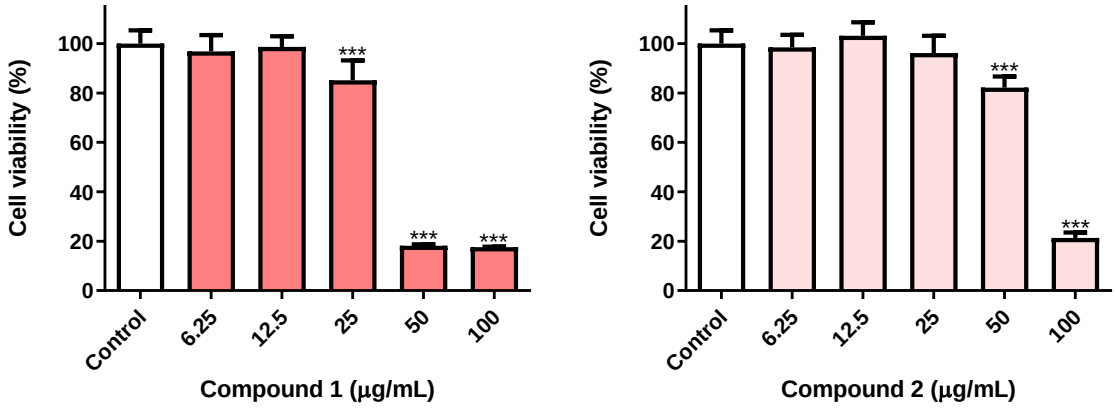

Fig. 2. Viability of *Sf9* cells exposed to the molecules **1** and **2** under study (6.25 – 100 µg/mL), medium (control). Cells were incubated for 72 h, after which viability was evaluated. *** $p < 0.001$.

2.2. Inverted Virtual Screening Results

The score obtained, for each SF, for compound **1** in complex all the possible targets, is depicted in Table 1. The range of values is different because the SFs are based on different metrics and scales. The GOLD SF are dimensionless, and a more positive value indicates a better binding affinity. AutoDock Vina, on the other hand, uses a system of measurement that is a more real approximation of the binding free energy, with a more negative score suggesting better affinity.

The results were ranked from best to worst. The PDB structure of each set of targets, that presented the best score, was selected as potential target. Compound **1** showed increased affinity toward acetylcholinesterase (AChE) and odorant binding protein 1 (OBP). The same tendency was observed for all the independent SF tested, reinforcing these conclusions.

Table 1. Scoring values of the eugenol derivative **1** obtained for all putative targets PDB structures with the five different scoring functions and overall ranking of the most likely protein targets for interaction.

Target	PDB	PLP	ASP	ChemScore	GoldScore	Vina	Overall Ranking
Acetylcholinesterase	**1QON**	81.19	59.26	37.75	69.05	-8.30	1
	1DX4	77.08	51.68	36.22	62.54	-7.70	
	4EY6	76.18	48.57	32.96	59.66	-7.60	
Alpha-esterase-7	**5TYJ**	59.68	33.92	32.74	54.09	-6.20	8
	5TYP	63.72	39.54	31.84	56.73	-6.20	
Beta-*N*-acetyl-D-hexosaminidase OfHex1	**3OZP**	71.22	49.42	29.92	63.78	-7.30	4
	3NSN	76.67	54.51	32.45	67.93	-6.50	
Chitinases	**3WQV**	68.53	49.59	31.24	65.25	-6.60	3
	3WL1	70.09	48.98	31.76	60.37	-7.00	

Preprints (www.preprints.org) | NOT PEER-REVIEWED | Posted: 5 August 2022 doi:10.20944/preprints202208.0126.v1

Ecdysone receptor (EcR)	**1R1K**	66.83	31.02	32.21	61.61	.7.70	5
	1R20	63.97	29.6	29.98	58.93	-6.80	
N-Acetylglucosamine-1-phosphate uridyltransferase (GlmU)	**2V0K**	58.12	28.56	23.72	59.67	-5.90	13
	2VD4	52.43	25.36	20.76	48.33	-5.20	
Octopamine receptor	**4N7C**	60.27	39.29	34.34	69.10	-5.90	7
Odorant Binding Protein	**2GTE**	70.46	39.20	30.71	66.39	-6.30	2
	3K1E	83.01	44.98	37.85	66.89	-5.90	
	5V13	80.20	49.37	40.18	63.84	-7.70	
	3N7H	74.95	39.20	30.71	66.39	-6.30	
Peptide deformylase	**5CY8**	72.08	30.11	25.48	71.01	-7.00	6
p-Hydroxyphenylpyruvate dioxygenase	**6ISD**	68.60	33.78	26.22	51.19	-7.00	9
Polyphenol oxidase (PPO)	**3HHS**	62.37	34.09	29.03	66.32	-5.70	11
Sterol carrier protein-2 (HaSCP-2)	**4UEI**	64.27	32.22	31.10	50.51	-6.20	10
Voltage-gated sodium channel	**6A95**	63.20	28.28	21.92	61.46	-6.10	12

2.3. Molecular Dynamics Simulations and Free Energy Calculations results

To evaluate the stability of the interactions formed between compound **1** and the two most probable targets predicted, AChE and OBP1, MD simulations were performed using the structure with the best score of these two groups, 1QON for AChE and 3K1E for OBP1. RMSD, solvent accessible surface area (SASA) and number of hydrogen bonds were the parameters calculated to evaluate the results, being depicted in Table 2. Overall, all the complexes and ligands present a low RMSD value, indicating that the systems are well equilibrated and stable. Compound **1** is buried into the pocket of both OBP1, with a percentage of potential ligand SASA buried values of 88% and a low ligand SASA (Figure S3 in Supplementary Material). When bound to AChE, it is more exposed to the solvent (percentage of potential ligand SASA buried values of 79%). This indicates that compound **1**, when in complex with OBP1, is highly protected from the solvent and well bound to the protein, throughout the simulation. Compound **1** is more exposed to the solvent, throughout the simulation, when in complex with AChE, mainly due to the exposure of the carboxylic portion of the molecule (as evidenced in Figure 1).

Hydrogen bond analysis allows the understanding of the interactions that occur between compound **1** and the possible targets throughout time. Globally, this compound maintains 0-1 hydrogen bonds, on average, with both OBP1 and AChE (Figure S4 in Supplementary Material).

Table 2 also shows the values for the Gibbs binding free energy of association calculated using MM/GBSA and highlights the three most important amino acid residues involved in the stabilization

Preprints (www.preprints.org) | NOT PEER-REVIEWED | Posted: 5 August 2022 doi:10.20944/preprints202208.0126.v1

of compound **1**. The average structure of the dominant cluster of AChE and OBP1 in complex with compound **1** is displayed in Fig. 3 and 4, respectively. These figures illustrate the details of the binding pocket and the interaction formed between the targets and compound **1**.

Table 2. Average protein and ligand RMSD values (Å), Average ligand SASA (Å^2), Percentage of Potential Ligand SASA buried, average number of ligand-target hydrogen bonds obtained from the MD simulations. ΔG binding energy determined using MM/GBSA and per-residue decomposition, calculated for the last 70 ns of the simulation.

	Average RMSD of the complex (Å)	**Average RMSD of the ligand (Å)**	**Ligand SASA (Å^2)**	**Percentage of Potential Ligand SASA buried (%)**	**Average Number H-bonds**	**ΔG_{bind} (kcal/mol)**	**Main Contributors (kcal/mol)**
AChE	3.4 ± 0.3	1.7 ± 0.4	111.2 ± 53.2	79	0.1 ± 0.2	-22.6 ± 0.2	Tyr71 (-2.3 ± 0.9) Trp321 (-1.6 ± 1.0) Tyr374 (-1.5 ± 0.8)
OBP1	2.1 ± 0.3	1.2 ± 0.2	63.7 ± 16.3	88	0.01 ± 0.1	-32.4 ± 0.2	Met91 (-1.3 ± 0.5) Gly92 (-1.8 ± 0.6) Trp114 (-2.5 ± 0.6)

Analyzing the Gibbs binding free energy of association, the results suggest that compound **1** has a higher affinity towards OBP1 than towards AChE (-32.4 kcal/mol *vs.* -22.6 kcal/mol). When bound to AChE, the compound is mainly stabilized through non-polar interactions with three aromatic residues, Tyr71 (-2.3 ± 0.9 kcal/mol), Trp321 (-1.6 ± 1.0 kcal/mol) and Tyr374 (-1.5 ± 0.8 kcal/mol). Regarding OBP1, compound **1** is stabilized through non-polar interactions with Met91 (-1.3 ± 0.5 kcal/mol) and Gly92 (-1.8 ± 0.6 kcal/mol) but can form a hydrogen bond with Trp114 (-2.5 ± 0.6 kcal/mol). Considering all the data presented, compound **1** seems to be a good candidate to be used as a repellent having OBP1 as its principal target.

Preprints (www.preprints.org) | NOT PEER-REVIEWED | Posted: 5 August 2022 doi:10.20944/preprints202208.0126.v1

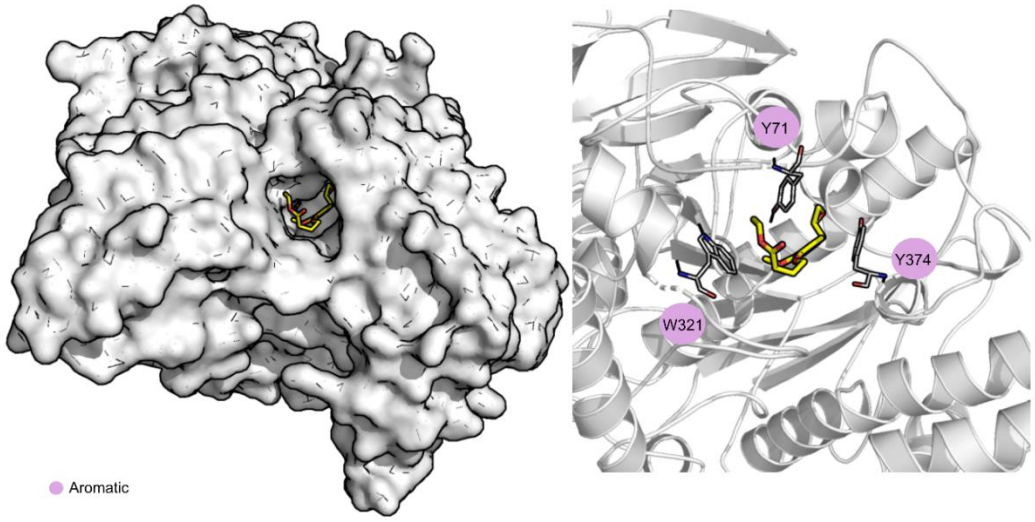

Fig. 3. Compound **1** bound to AChE. Surface and cartoon representation. Compound **1** represented in yellow licorice.

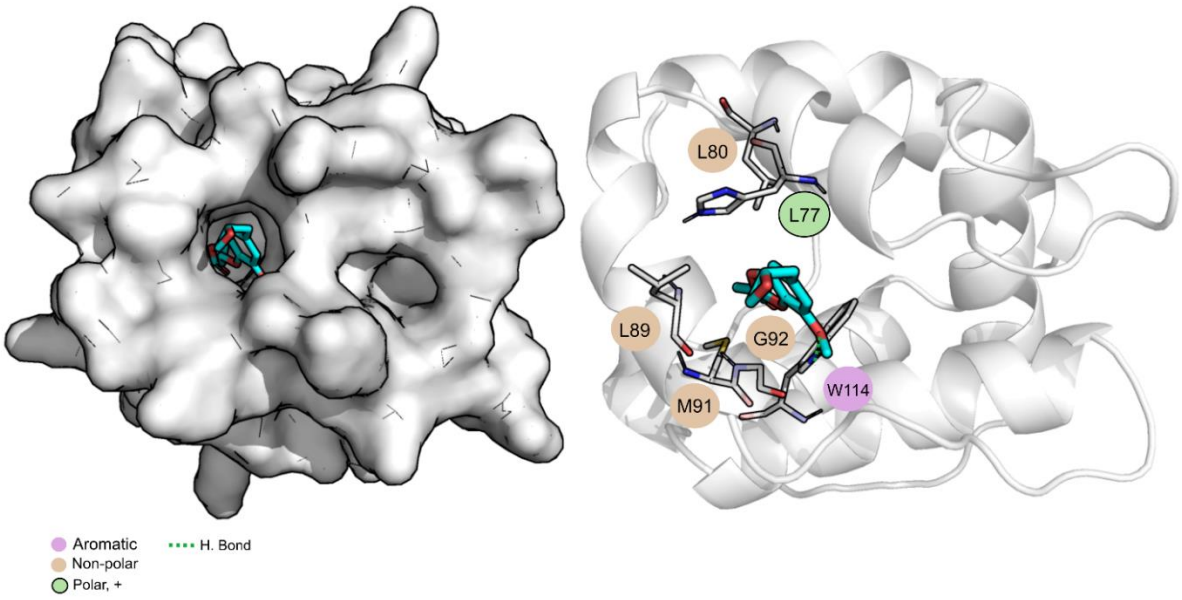

Fig. 4. Compound **1** bound to OBP1. Surface and cartoon representation. Compound **1** in cyan licorice.

2.4. Encapsulation assays

Compound **1** was encapsulated into liposomes of Egg-PC:Ch (7:3) and DOPG (100 %) aiming at obtaining a high encapsulation efficiency and effective release. The ethanolic injection method was chosen considering previous results of release profiles of eugenol, carvacrol and thymol derivatives [11,12]. The lipid components of the liposomes determine the rigidity, fluidity and surface charge and, consequently, their ability to be loaded with bioactive compounds and release them [13]. For instance, the use of unsaturated lipids, such as phosphatidylcholines from natural sources (egg or soy lecithin), results in relatively permeable liposomes [14]. On the other hand, cholesterol molecules are also known to modulate membrane rigidity properties. Liposomes of Egg-PC:Ch (70:30) have been

used as bilayer models in membrane permeation assays [15,16]. DOPG, a main component of pulmonary surfactant, forms negatively-charged liposomes in a liquid-crystalline phase, due to its low transition temperature of -18 °C [17,18].

Prior to encapsulation studies, absorption and fluorescence emission of compound **1** in solution was measured and the corresponding spectra are displayed in Figure S5 in Supplementary Material. An absorption maximum at 280 nm was observed and a fluorescence band between 290 nm and 390 nm was detected, with maximum emission around 320 nm. These properties allow using compound fluorescence to determine the encapsulation efficiencies and release profiles. High encapsulation efficiencies of compound **1** were obtained (Table 3), showing that both formulations are able to encapsulate this molecule at concentrations that may guarantee a biological activity. Nonetheless, liposomes of Egg-PC:Ch (70:30) have shown to be more efficient to encapsulate compound **1**, presenting higher encapsulation efficiency than DOPG liposomes.

Table 3. Encapsulation efficiency, EE(%) ± SD(%), of compound **1** in liposomes (SD: standard deviation).

Liposomes	EE(%) ± SD(%)
Egg-PC:Ch (70:30)	88.8 ± 2.7
DOPG (100 %)	79.8 ± 2.6

Liposomes stability is an important key for their application. Therefore, a stability study was performed measuring structural parameters like the hydrodynamic diameter, polydispersity index (PDI) and zeta potential along time (Fig. 5).

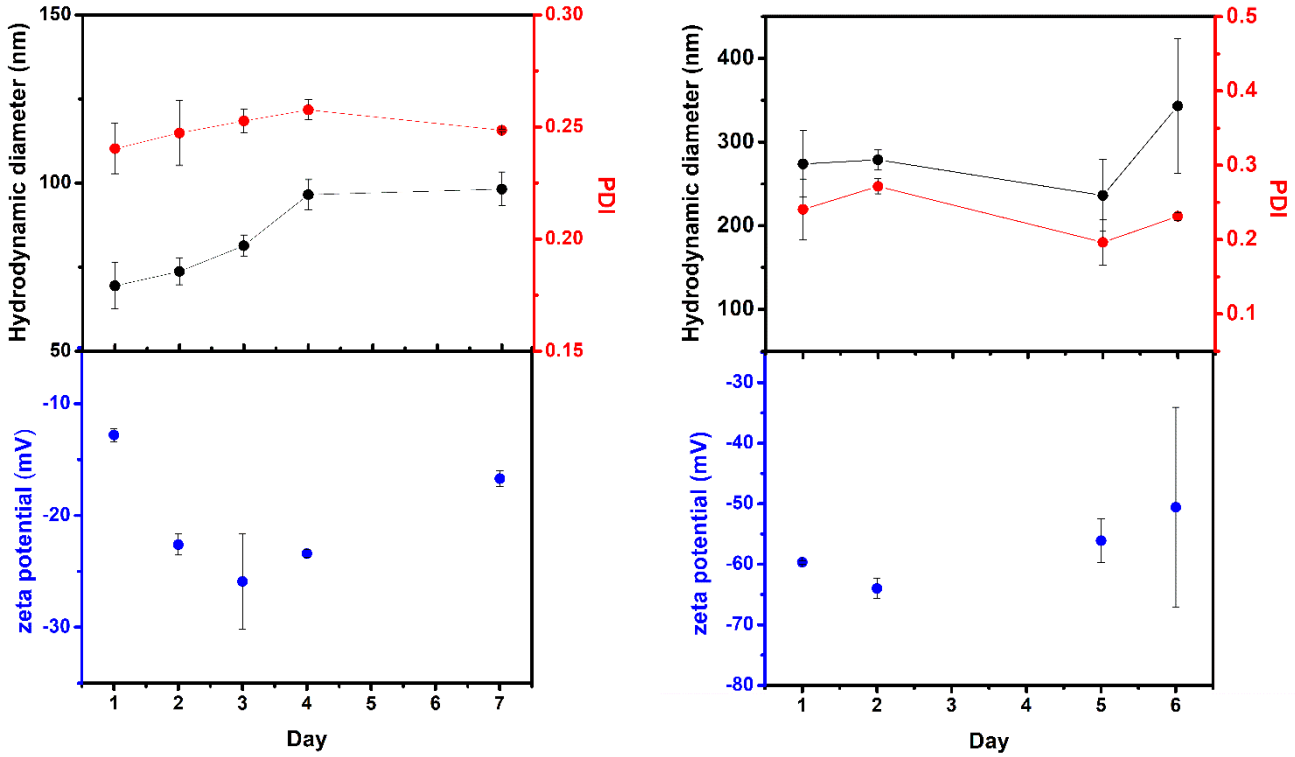

Preprints (www.preprints.org) | NOT PEER-REVIEWED | Posted: 5 August 2022 doi:10.20944/preprints202208.0126.v1

Fig. 5. Hydrodynamic diameter, polydispersity index (PDI), and zeta potential of Egg-PC:Ch (7:3) (left), and 100% DOPG (right) liposomes (error bars represent SD from three independent measurements).

In general, liposomes of Egg-PC:Ch and DOPG have shown to be generally stable for 7 and 6 days, respectively. The loaded nanoformulation of Egg-PC:Ch exhibit structures much smaller in size, comparing to the DOPG one, in accordance with previous results of liposomal formulations based on Egg-PC [19]. Along 7 days, Egg-PC:Ch liposomes size increased from 70 nm to *ca.* 95 nm (Fig. 5 – left), a tendency also previously observed in these nanosystems [19], due to their almost neutral charge (very slightly negative zeta potential), pointing to some aggregation. Nevertheless, the loaded liposomes maintain a small size and a low polydispersity index over a week. Compound **1**-loaded DOPG liposomes display much larger hydrodynamic diameters of around 280 nm, increasing its size to 340 nm after 6 days, with a small PDI value. The charge repulsion between the negatively-charged phosphate groups (the glycerol moiety in the lipid polar head is neutral) justifies the larger diameters and the overall tendency for a lower aggregation, due to the strongly negative zeta potential (Fig. 5 – right).

Cumulative release of compound **1** from the two liposomal formulations was also assessed and the experimental data of release profiles were fitted to the first-order kinetic model (Figure S6 in Supplementary Material) and to the Weibull model (Fig. 6). The values of the models' parameters are summarized in Table 4.

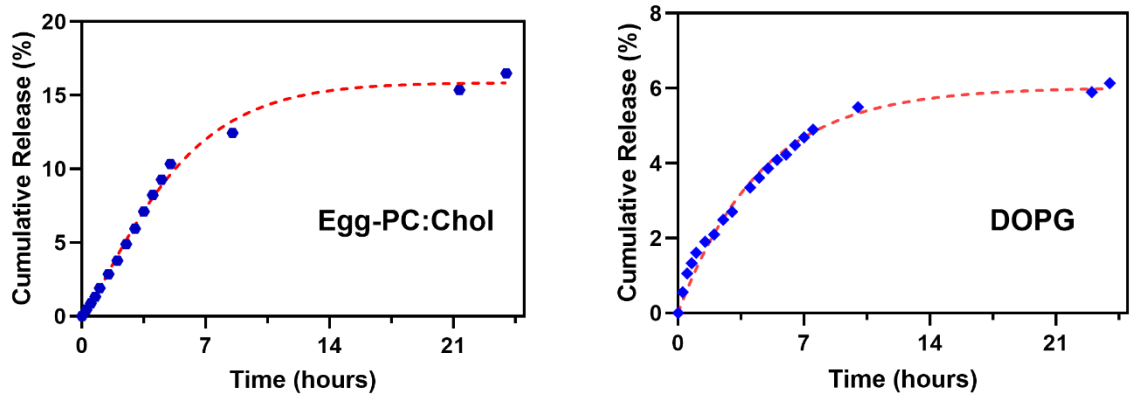

Fig. 6. Cumulative release of compound **1** from liposomes of Egg-PC:Cholesterol (left) and DOPG (right) liposomes fitted to the Weibull model.

Quite similar release profiles were obtained for both liposomal formulations, with an initial burst release followed by a slower decay. Egg-PC:Ch liposomes present a slower compound leakage in the early stage of release than DOPG liposomes. However, after 24 h, the release from DOPG liposomal formulation is very small, showing a retention of the compound by these liposomes.

Preprints (www.preprints.org) | NOT PEER-REVIEWED | Posted: 5 August 2022 doi:10.20944/preprints202208.0126.v1

Table 4. Parameters obtained by fitting the release profiles to the first-order kinetic model and Weibull model, and the respective coefficients of determination (R^2).

	First-order kinetics		Weibull		
	k	***R²***	***b***	***a***	***R²***
Egg-PC:Ch	0.16	0.988	0.1258	1.244	0.995
DOPG	0.21	0.985	0.2469	0.8457	0.9904

The best-fitting model describing compound **1** release from liposomes was the Weibull model, with higher coefficients of determination for both liposomal formulations (Table 4), and pointing to a compound release by Fickian diffusion (*b* values below 0.75 in both formulations [20]). Nevertheless, the fit to the first-order kinetic model also shows a good correlation (Table 4).

Considering the very high encapsulation efficiency (almost 90%) of compound **1** in Egg-PC:Ch liposomes and the release profile, together with a good stability of the compound-loaded nanosystem, this formulation was chosen for the subsequent assays of insecticidal activity.

*2.5 Compound **1**-loaded liposomes maintained insecticidal activity, while decreased toxicity towards human cells*

Considering the encapsulation efficiency and release profile, the liposomes were loaded with compound **1**, to obtain the concentration equivalent to 100 µg/mL. To find out if the nanoformulation maintained the cytotoxicity towards *Sf9* cells, compound **1**-loaded liposomes were compared (side-by-side) with compound **1** in another set of experiments (Fig. 7, left). With this aim in view, we firstly explored the putative impact that drug-free liposomes may have on cell viability, and it has been proved that they have no effect on the viability of the cells under study (*Sf9* cell and HaCaT cells) (Figure S7 in Supplementary Material). The cytotoxicity of compound **1** and compound **1**-loaded liposomes is depicted in Fig. 7. It has been proved that the encapsulation of compound **1** in liposomes did not conduct to a loss of toxicity towards *Sf9* cells (Fig. 7, left), which is a promising finding. Furthermore, bearing in mind the importance of developing formulations that have a safer toxicological profile and considering the usual routes of pesticides poisoning, specifically skin, cytotoxicity towards keratinocytes (HaCaT cells) was explored. Noteworthy, the encapsulation of compound **1** into liposomes led to a significant decrease in toxicity towards human cells of nearly 20% at the highest concentration tested (100 µg/mL) (Fig. 7, right).

Preprints (www.preprints.org) | NOT PEER-REVIEWED | Posted: 5 August 2022 doi:10.20944/preprints202208.0126.v1

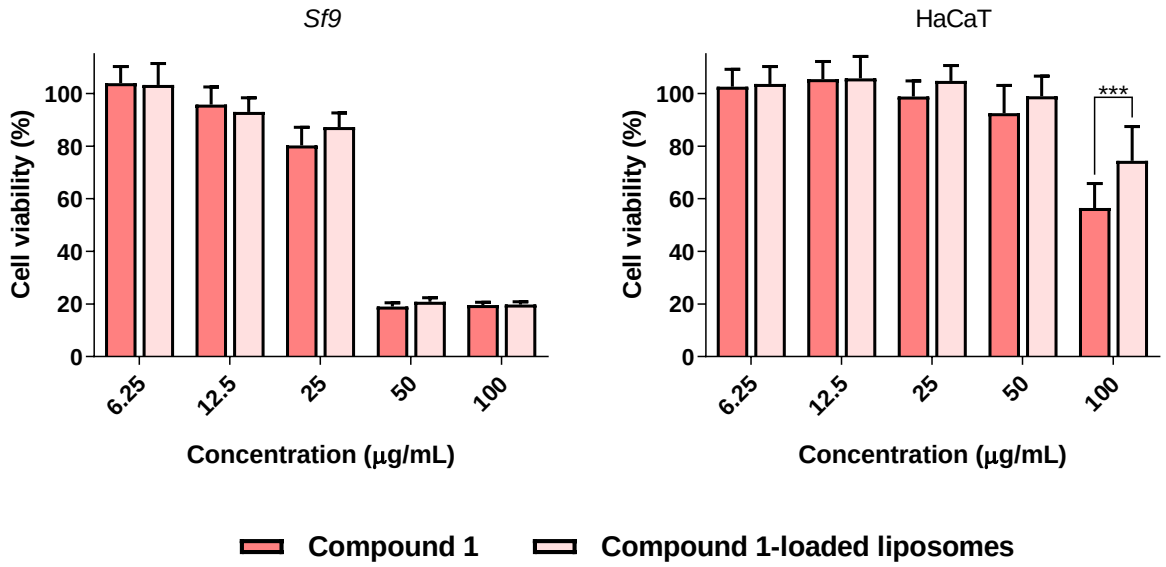

Fig. 7. Viability of *Sf9* and HaCaT cells exposed to compound **1** and compound **1**-loaded liposomes (6.25 – 100 µg/mL). Cells were incubated for 72 h, after which viability was evaluated. *** $p < 0.001$.

3. Conclusions

Ethyl 4-(2-methoxy-4-(oxiran-2-ylmethyl)phenoxy)butanoate **1**, an eugenol active derivative, was encapsulated in liposomes of Egg-PC:cholesterol (7:3) and 100% DOPG, with very high encapsulation efficiencies. The compound-loaded liposomes are generally stable for 6-7 days, the Egg-PC:Ch nanosystem providing a more effective release. This formulation was chosen for biological assays, and the results showed that the encapsulation of compound **1** in liposomes did not conduct to a loss of toxicity towards insecticidal activity in *Sf9* cells, and led to a significant decrease in toxicity towards human cells, specifically keratinocytes (HaCaT cells) cells of nearly 20% at the highest concentration tested (100 µg/mL), which are promising finding for future application of compound **1** as insecticide.

The most likely targets were predicted, and the stability of the complex confirmed using in *silico methods*, including structure-based inverted virtual screening and molecular dynamics simulations. Free energy calculations were used to estimate the binding free energy and provide a detailed characterization of the binding mode. Insect acetylcholinesterase and/or odorant binding proteins are, most likely, the targets of this compound since the resulting complexes exhibit appropriate predicted binding affinity and are stable throughout the simulation time.

4. Methods and materials

4.1. Cell culture

Preprints (www.preprints.org) | NOT PEER-REVIEWED | Posted: 5 August 2022 doi:10.20944/preprints202208.0126.v1

Sf9 (*Spodoptera frugiperda*) cells were maintained as a suspension culture and cultivated in Grace's medium with 10% fetal bovine serum (FBS) and 1% penicillin/streptomycin, at 28 ºC. Cells were used in experiments while in the exponential phase of growth. On the other hand, HaCaT (human keratinocyte) cells were cultured in Dulbecco's Modified Eagle Medium (DMEM) supplemented with 10% FBS and 1% penicillin/streptomycin at 37 ºC, in a humidified atmosphere of 5% CO_2.

4.2. Viability assessment

For the assessment of viability, a resazurin-based method was used. The *Sf9* and HaCaT cells were plated at a density of 1.5×10^4 and 5.0×10^3 cells/well, respectively, incubated for 24 h, and then exposed to the molecules under study (at 6.25 – 100 µg/mL in Grace's medium) for 72 h. After this period, a commercial solution of resazurin was added (1:10), and the kinetic reaction of fluorescence increase was monitored at 560/590 nm. For HaCaT and the *Sf9* cells, 30 and 60 min of incubation were used, respectively.

4.3. Inverted Virtual Screening (IVS) studies

A search on *Scopus* was performed for papers describing virtual screening (VS) studies involving targets and molecules with insecticidal activity. The selection criteria were relevance of the target and year of publication. In the seventeen studies found, thirteen targets and twenty-three crystallographic structures were identified and are listed in Table 5.

Table 5. List of targets selected for the inverted virtual screening study

Target	Organism	PDB target	Resolution (Å)	Description	Ref.
Ecdysone receptor	*Heliothis virescens*	1R20	3.00	VS based on 1R20 bound to an agonist as a model for the development of a receptor-based pharmacophore model.	[21]
		1R1K	2.90	VS of 2 million compounds against 1R1K, an ecdysone receptor structure bound to its known ligand ponasterone A.	[22]
Chitinase	*Ostrinia furnacalis*	3WL1	1.77	Pharmacophore-based screening using two crystal structures of chitinases: 3WL1 bound to its reaction product and 3WQV bound to an inhibitor.	[23]
		3WQV	2.04		
β -*N*-Acetyl-D-hexosaminidase OfHex1		3NSN	2.10	VS of the ZINC database to identify OfHex1 inhibitors using 3NSN crystal structure bound to a known inhibitor.	[24]
		3OZP	2.00	VS of the ZINC data-	[25]

Preprints (www.preprints.org) | NOT PEER-REVIEWED | Posted: 5 August 2022 doi:10.20944/preprints202208.0126.v1

				base targeting 3OZP, a crystal structure of OfHex1 bound to an inhibitor.	
***N*-Acetylglucosamine-1-phosphate uridyltransferase (GlmU)**	*Xanthomonas oryzae*	2V0K	2.30	Homology model built for docking using 2V0K and 2VD4 as templates. 2V0K crystal structure is bound to its known ligand and 2VD4 is bound to a possible inhibitor.	[26]
		2VD4	1.90		
Acetylcholinesterase	*Aedes aegypti*	1QON	2.72	Search for new molecules with insecticidal activity against *Ae. Aegypti* using acetylcholinesterase crystal structures 1QON and 4EY6 as targets, both bound to possible inhibitors.	[27]
		4EY6	2.40		
	Drosophila melanogaster	1DX4	2.70	Homology 3D model built for VS using 1DX4 as template. 1DX4 crystal structure is bound to a potent inhibitor.	[28]
Polyphenol oxidase	*Manduca sexta*	3HSS	2.70	Crystal structure of a prophenoloxidase from *Manduca sexta*.	[29]
***p*-Hydroxyphenylpyruvate dioxygenase**	*Arabidopsis thaliana*	6ISD	2.40	Development of a receptor-ligand pharmacophore model based on the crystal structure 6ISD bound to a commonly used pesticide. The best model created was then used for VS studies.	[30]
Voltage-gated sodium channel	*Periplaneta americana*	6A95	2.60	Crystallographic structure of a Voltage-gated sodium channel NavPaS bound to a pore blocker, tetrodotoxin (TTX)	[31]
Octopamine receptor	*Blattella germanica*	4N7C	1.75	Crystal structure of Bla g 4, an octopamine receptor, bound to tyramine.	[32]
Sterol carrier protein-2 (HaSCP-2)	*Helicoverpa armigera*	4UEI	Solution NMR	Structure-based VS of a database of commercially available compounds to find potential inhibitors of HaSCP-2. The residues Phe53, Thr128, and Gln131 were selected for the binding cavity.	[33]
Peptide deformylase	*Xanthomonas oryzae*	5CY8	2.38	Docking and VS of a library of 318 phytochemicals. 5CY8 crystal structure is bound to a possible inhibitor.	[34]
Alpha-esterase-7 (αE7)	*Lucilia cuprina*	5TYJ	1.75	Computational design of potent and selective covalent inhibitors of αE7. 5TYJ and 5TYP crystal structures are bound to inhibitors: (3-bromo-5-	[35]
		5TYP	1.88		

Preprints (www.preprints.org) | NOT PEER-REVIEWED | Posted: 5 August 2022 doi:10.20944/preprints202208.0126.v1

				phenoxylphenyl)boronic acid and (3-bromo-4-methylphenyl)boronic acid, respectively.	
Odorant Binding Protein	*Aedes aegypti*	5V13	1.84	Search for new molecules with insecticidal activity against *Ae. Aegypti* using a crystal structure of a mosquito juvenile hormone-binding protein, 5V13 bound to its natural hormone.	[27]
	Drosophila melanogaster	2GTE	1.40	2GTE crystal structure is bound to its natural ligand	[36]
	Anopheles gambiae	3N7H	1.60	QSAR and docking studies for the rational design of mosquito repellents using the crystal structure 3K1E bound to a polyethylene glycol molecule. 3N7H crystal structure is bound to a commonly used repellent.	[37]
	Aedes aegypti	3K1E	1.85		[37]

Each target was prepared for IVS using pymol [38]. The crystallographic ligands, when present, were extracted from the respective targets and saved for binding site reference and posterior validation. When no ligand was present, the binding site was inferred from the bibliography, and the most important amino acid residues were considered. To validate the protocol, re-docking was used. It consists in removing the crystallographic ligand and re-docking it with the docking scoring functions (SFs) to evaluate their ability to reproduce the orientation and position of the ligand. The results are measured in terms of root mean square deviation (RMSD) between the predicted pose and the reference position in the crystallographic structure, with a value below 2 Å being a measure of good protocol quality.

For this study, five scoring functions were used: PLP, ASP, ChemScore and GoldScore (all part of the GOLD [39] software) and AutoDock Vina [40]. The docking conditions were equivalent across all the SFs to ensure consistency and reproducibility. The conditions that performed the best were then applied at the IVS stage. The optimized parameters consisted of docking coordinates and box dimension (or radius in the case of GOLD), number of runs and exhaustiveness or search efficiency. The chemical structure of the eugenol derivative **1** was prepared using Datawarrior [41] and OpenBabel [42]. Compound **1** was docked into each target with all the SF and a list of ranked scores were created. This protocol is well established and has been applied to other IVS studies involving other eugenol and carvacrol derivatives [11,12].

4.4. Molecular Dynamics Simulations and Free Energy Calculations

Preprints (www.preprints.org) | NOT PEER-REVIEWED | Posted: 5 August 2022 doi:10.20944/preprints202208.0126.v1

The IVS predictions were confirmed performing molecular dynamics simulations (MD) on the most promising targets predicted: Acetylcholinesterase (PDB: 1QON) and Odorant binding protein 1 (PDB: 3K1E). Since, for MD simulations the protein structures must not present any gaps, a homology model was created using SWISSMODEL [43] (Figure S1 in Supplementary Material). The ligand pose used in the MD simulations were the ones predicted with GOLD/PLP scoring function, posteriorly treated with the Leap module of AMBER [44]. The predicted targets, 1QON and 3K1E were treated with the ff14SB force field [45] and compound **1** was parameterized using ANTECHAMBER, with the General Amber Force Field (GAFF) [46], with the RESP HF/6-31G(d) charges calculated with Gaussian16 [47]. Sodium counter ions (Na^+) were added to neutralize the charge of the system and the protein-ligand complexes were placed in TIP3P water box with 12 Å distance between the surface of the protein and the side of the box, with periodic boundary conditions. The long-range electrostatic interactions were calculated using the particle mesh Ewald summation method. The cut-off value for the short-range electrostatic and Lennard-Jones interactions was set at 10.0 Å. The SHAKE algorithm was used to constrain the hydrogen bonds and a time step of 2 fs was employed.

In this MD protocol, the 100 ns production run was preceded by four minimization steps and two equilibration steps. The four consecutive minimization stages were applied, to remove clashes and were applied to the following groups of atoms: 1-water molecules (2500 steps); 2-hydrogens atoms (2500 steps); 3-side chains of all the amino acid residues (2500 steps); 4-full system (10000 steps). The fist equilibration was performed in a NVT ensemble, where the systems were heated to 298 K applying a Langevin thermostat at constant volume (50 ps). In the second equilibration step, the density of the systems was further equilibrated at 298 K (subsequent 50 ps). Finally, the production run was performed using an NPT ensemble at constant temperature (298 K), pressure (1 bar, Berendsen barostat).

The final trajectory obtained for each target was analyzed using the cpptraj tool [48] of AMBER and VMD [49]. RMSD, number of hydrogen bonds formed, and accessible surface area were the parameters calculated to evaluate the stability of the protein-ligand complexes. This overall procedure is robust and has been previously used with success in the treatment of several biomolecular systems [50-53].

The Molecular Mechanics - Generalized Born Surface Area (MM-GBSA) method [54] was applied to present an estimation of the binding free energies of compound **1** when in complex with acetylcholinesterase and the odorant binding protein 1. A salt concentration of 0.100 $mol.dm^{-3}$ was used and the contribution of the amino acid residues was accessed applying the energy decomposition method to each complex. From each MD trajectory, a total of 1400 conformations taken from the last 70 ns of simulation were considered for the MM-GBSA calculations.

Preprints (www.preprints.org) | NOT PEER-REVIEWED | Posted: 5 August 2022 doi:10.20944/preprints202208.0126.v1

4.5. Nanoencapsulation studies and release assays

Compound **1**, ethyl 4-(2-methoxy-4-(oxiran-2-ylmethyl)phenoxy)butanoate, was used for nanoencapsulation studies in liposomes of 1,2-diacyl-*sn*-glycero-3-phosphocholine from egg yolk (egg phosphatidylcholine, Egg-PC)/cholesterol (Ch) (70% Egg-PC, 30% Ch) and of 100% 1,2-dioleoyl-*sn*-glycero-3-[phospho-*rac*-(1-glycerol)] (dioleoylphosphatidylglycerol, DOPG) (lipid structures in Fig. 8).

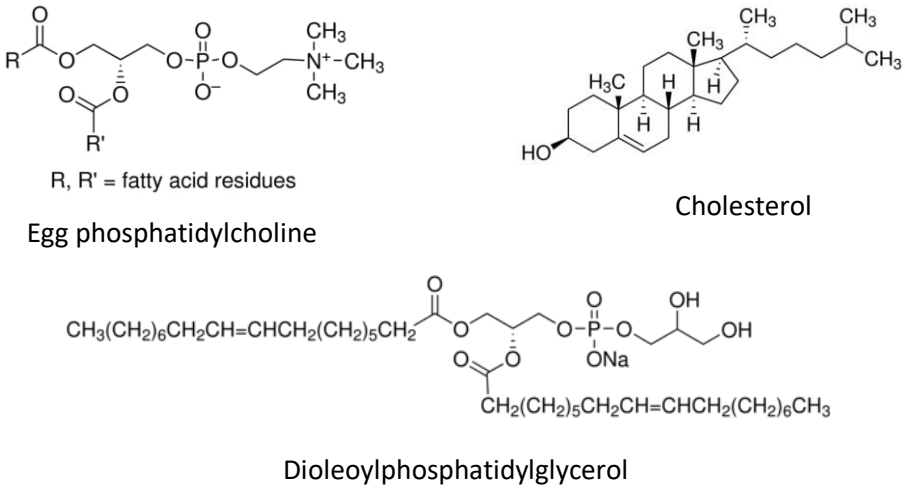

Fig. 8. Structure of the lipids used in liposomal formulations.

The ethanolic injection method was employed to prepare the liposomes. For that, an ethanolic solution of lipids and compound **1** was slowly injected into an aqueous solution, under vortexing [55]. The encapsulation efficiency, *EE* (%), was obtained through Equation (1),

$$EE(\%) = \frac{Total\ amount - Amount\ of\ non{-}encapsulated\ compound}{Total\ amount} \times 100 \quad (1)$$

The amount of non-encapsulated compound was isolated from the compound-loaded liposomes resorting to Amicon® Ultra centrifugal filter units of 100 kDa, by centrifugation at 3000 rpm for 10 minutes. After centrifugation, the filtrate (containing the non-encapsulated compound) was pipetted out and the fluorescence spectrum was measured. The maximum fluorescence intensity allowed to determine the concentration of non-encapsulated compound, using a previously obtained calibration curve (fluorescence intensity *vs.* concentration). Fluorescence spectra were measured in a Fluorolog 3 spectrofluorometer and three independent assays were carried out for determination of the encapsulation efficiency in each liposomal formulation. UV-Vis absorption spectrum of compound **1** was obtained in a Shimadzu UV-3600 Plus UV-Vis-NIR spectrophotometer.

Preprints (www.preprints.org) | NOT PEER-REVIEWED | Posted: 5 August 2022 doi:10.20944/preprints202208.0126.v1

The structural characterization and stability of liposomes was evaluated by Dynamic Light Scattering (DLS), using a Litesizer 500 equipment from Anton Paar, with a solid-state laser of 648 nm and 40 mW. For the hydrodynamic diameter and zeta potential measurements of the compound-loaded liposomes, three independent measurements (at 25 °C) were performed.

Release assays from the compound-loaded liposomes were carried out using Amicon® Ultra-0.5 mL centrifugal filters with 0.1 µm pore size. The upper part of the filter was filled with the compound-loaded liposomes, while the bottom was filled with a phosphate buffer solution (pH = 7). Along the time of the experiment, 200 µL aliquots were collected from the bottom compartment, and an equal volume of fresh buffer was added, to determine the cumulative compound release. The fluorescence intensity of the aliquots was measured, and the release kinetics was fitted to the first-order kinetic model [56] and to Weibull model [20].

The first-order kinetic model follows Equation (2),

$$F(\%) = M_0 \times (1 - e^{-kt}) \quad (2)$$

where *F(%)* is the percentage of released compound, M_0 represents the total amount of compound released, *k* represents the first-order rate constant and *t* the time.

The Weibull model is a distribution function, which expresses the compound fraction accumulated (*m*) in solution on time *t*, following Equation (3),

$$m = 1 - \exp\left[\frac{-(t-T_i)^b}{a}\right] \quad (3)$$

where *a* is a parameter defining the timescale of the process, T_i a location parameter representing the latency time of the release mechanism (considered zero many times) and *b* denotes the curve type shape parameter. For $b > 1$, the transport follows a complex release mechanism; $b \leq 0.75$ indicates Fickian diffusion (in either fractal or Euclidian spaces); $0.75 < b < 1$ indicates a combined mechanism (Fickian diffusion and Case II transport) [20].

4.6. Statistical analysis

For biological assays, the Shapiro–Wilks normality test was performed in the data to ensure that it followed a normal distribution. Comparison between the means of controls and each experimental condition was performed using ordinary one-way ANOVA – Dunnett's multiple comparisons test. Comparison between the means of encapsulated and non-encapsulated compound **1** was done using two-way ANOVA – Tukey's multiple comparisons test. Outliers were identified by the Grubbs' test. Data was expressed as the mean ± standard deviation (SD) of at least three independent experiments. GraphPad Prism 8.0 software was used, and values were considered statistically significant when $p < 0.05$.

Funding: This research was funded by project PTDC/ASP-AGR/30154/2017 (POCI-01-0145-FEDER-030154) of the COMPETE 2020 program, co-financed by the FEDER and the European Union. The authors acknowledge also the Foundation for Science and Technology (FCT, Portugal) and FEDERCOMPETE-QREN-EU for financial support to the research centers CQ-UM (UID/QUI/00686/2021), CF-UM-UP (UIDB/04650/2020) and REQUIMTE (UIDB/50006/2020). Renato B. Pereira acknowledges PRIMA Foundation (H2020-PRIMA 2018—Section 2, Project MILKQUA) and FCT (PTDC/QUI-QFI/2870/2020) for the funding. The NMR spectrometer Bruker Avance III 400 is part of the National NMR Network and was purchased within the framework of the National Program for Scientific Re-equipment, contract REDE/1517/RMN/2005 with funds from POCI 2010 (FEDER) and FCT.

Conflicts of interest/Competing interests: The authors declare that they have no conflict of interest.

Supplementary Material

The Supporting Information is available free of charge via the Internet. Supplementary figures (Figure S1. Homology model built for 1QON. Green is the original structure and red represents the loop that was generated by SWISS-MODEL. In orange is the ligand molecule (compound **1**). GMQE - Global Model Quality Estimation, is expressed between 0 and 1 with a higher number meaning higher reliability. QMEAN - provides an estimate of the "degree of nativeness" of the structural features observed in the model. A value of QMEAN around zero indicate a good agreement between the model and experimental structure. Figure S2. Protein and ligand RMSD (Å) of the AChE and OBP – ligand complexes. Figure S3. Percentage of the potential solvent accessible surface area of the ligands that is buried by the protein targets evaluated. Figure S4. Number of ligand-target hydrogen bonds formed during the simulations for compound **1** when complexed with AChE and OBP. Figure S5. Normalized absorption and fluorescence emission (excitation at 280 nm) spectra of compound **1** in ethanol (1×10^{-5} M for absorption and 1×10^{-6} M for emission). Figure S6. Cumulative release of compound **1** from liposomes of Egg-PC:Cholesterol (left) and DOPG (right) liposomes fitted to the first-order kinetic model. Figure S7. Viability of *Sf9* and HaCaT cells exposed to drug-free liposomes (6.25 – 100 µg/mL), medium (control). Cells were incubated for 72 h, after which viability was evaluated).

Author Information

Corresponding Author: *M. Sameiro T. Gonçalves, 00351253604372, msameiro@quimica.uminho.pt

Abbreviations

AChE: acetylcholinesterase; DLS: dynamic light scattering; DMEM: Dulbecco's Modified Eagle Medium; DOPG: dioleoylphosphatidylglycerol; Egg-PC:Ch: egg-phosphatidylcholine/cholesterol; EE: Encapsulation efficiency; FBS: fetal bovine serum; HaCaT: human keratinocyte cells; ^{1}H NMR: Proton nuclear magnetic resonance; IVS: inverted virtual screening; MD: molecular dynamics simulations; MM-GBSA: molecular mechanics - generalized born surface area; OBP: odorant binding protein 1; RMSD: root mean square deviation; SASA: solvent accessible surface area; *Sf*9: *Spodoptera frugiperda*; SFs: scoring functions.

References

] A. Khallaf, P. Wang, S. Zhuo, H. Zhu, H. Liu, Synthesis, insecticidal activities, and structure–activity relationships of 1,3,4-oxadiazole-ring-containing pyridylpyrazole-4-carboxamides as novel insecticides of the anthranilic diamide family, *J. Heterocycl. Chem.* 58 (2021) 2189-2202. https://doi.org/10.1002/jhet.4346

[2] C.A.G. da Camara, B. Doboszewski, J.P.R. de Melo, A.Y. Nazarenko, R.B. dos Santos, M.M. Moraes, Novel insecticides from alkylated and acylated derivatives of thymol and eugenol for the control of Plutella xylostella (*Lepidoptera: Plutellidae*), *J. Braz. Chem. Soc.* 33 (2022) 196-204. https://doi.org/10.21577/0103-5053.20210137

[3] M.J.G. Fernandes, R.B. Pereira, D.M. Pereira, A.G. Fortes, E.M.S. Castanheira, M.S.T. Gonçalves, New eugenol derivatives with enhanced insecticidal activity, *Int. J. Mol. Sci.* 21 (2020) 9257. https://doi.org/10.3390/ijms21239257

[4] A. El Asbahani, K. Miladi, W. Badri, M. Sala, E.H. Aït Addi, H. Casabianca, A. El Mousadik, D. Hartmann, A. Jilale, F.N. Renaud, A. Elaissari, Essential oils: from extraction to encapsulation. *Int. J. Pharm.* 483 (2015) 220-243. https://doi.org/10.1016/j.ijpharm.2014.12.069

[5] E. Pinho, M. Grootveld, G. Soares, M. Henriques, Cyclodextrins as encapsulation agents for plant bioactive compounds. *Carbohydr. Polym.* 101 (2014) 121–135. https://doi.org/10.1016/j.carbpol.2013.08.078

[6] U. Bulbake, S. Doppalapudi, N. Kommineni, W. Khan, Liposomal formulations in clinical use: An updated review. *Pharmaceutics.* 9 (2017) 12. 10.3390/pharmaceutics9020012

[7] F. Shi, J.-H. Zhao, Y. Liu, Z. Wang, Y.-T. Zhang, N.-P. Feng, Preparation and characterization of solid lipid nanoparticles loaded with frankincense and myrrh oil. *Int. J. Nanomedicine* 7 (2012) 2033–2043. https://doi.org/10.2147/IJN.S30085

[8] C.C. Liolios, O. Gortzi, S. Lalas, J. Tsaknis, I. Chinou, Liposomal incorporation of carvacrol and thymol isolated from the essential oil of *Origanum dictamnus* L. and *in vitro* antimicrobial activity. *Food Chem.* 112 (2009) 77–83. https://doi.org/10.1016/j.foodchem.2008.05.060

[9] S. Varona, A. Martín, M.J. Cocero, Liposomal incorporation of lavandin essential oil by a thin-film hydration method and by particles from gas-saturated solutions. *Ind. Eng. Chem. Res*. 50 (2011) 2088–2097. https://doi.org/10.1021/ie102016r

[10] M. Nuruzzaman, M.M. Rahman, Y. Liu, R. Naidu, Nanoencapsulation, nano-guard for pesticides: A new window for safe application. *J. Agric. Food Chem.* 64 (2016) 1447–1483. https://doi.org/10.1021/acs.jafc.5b05214

[11] R.B. Pereira, N.F.S. Pinto, M.J.G. Fernandes, T.F. Vieira, A.R.O. Rodrigues, D.M. Pereira, S.F. Sousa, E.M.S. Castanheira, A.G. Fortes, M.S.T. Gonçalves. Amino alcohols from eugenol as potential semisynthetic insecticides: chemical, biological, and computational insights. *Molecules* 26 (2021) 6616. https://doi.org/10.3390/molecules26216616

[12] M. Natal, M.J.G. Fernandes, N.F.S. Pinto, R.B. Pereira, T.F. Vieira, A.R.O. Rodrigues, D.M. Pereira, S.F. Sousa, A.G. Fortes, E.M.S. Castanheira, M.S.T. Gonçalves. New carvacrol and thymol derivatives as potential insecticides: synthesis, biological activity, computational studies and nanoencapsulation. *RSC Adv*. 11 (2021) 34024–34035. https://doi.org/10.1039/d1ra05616f

[13] A.M.S Simão, M. Bolean, T.A.C Cury, R.G. Stabeli, R. Itri, P. Ciancaglini. Liposomal systems as carriers for bioactive compounds. *Biophys Rev*. 7 (2015) 391-397. https://doi.org/10.1007/s12551-015-0180-8

[14] A. Kondratowicz, M. Weiss, W. Juzwa, Ł. Majchrzycki, G. Lewandowicz. Characteristics of liposomes derived from egg yolk. *Open Chemistry* 17 (2019) 763-778. https://doi.org/10.1515/chem-2019-0070

[15] M. Crisma, A. Barazza, F. Formaggio, B. Kaptein, Q.B. Broxterman, J. Kamphuis, C. Toniolo. Peptaibolin: synthesis, 3D-structure, and membrane modifying properties of the natural antibiotic and selected analogues. *Tetrahedron* 57 (2001) 2813-2825. https://doi.org/10.1016/S0040-4020(01)00124-7

[16] V.I.B. Castro, C.M Carvalho, R.V.D. Fernandes, S.M.M.A Pereira-Lima, E.M.S Castanheira, S.P.G. Costa. Peptaibolin analogues by incorporation of α,α-dialkylglycines: synthesis and study of their membrane permeating ability. *Tetrahedron* 72 (2016) 1024-1030. https://doi.org/10.1016/j.tet.2015.12.079

[17] J.S. Vincent, S.D. Revak, C.D. Cochrane, I.W. Levin. Interactions of model human pulmonary surfactants with a mixed phospholipid bilayer assembly: Raman spectroscopic studies. *Biochemistry* 32 (1993) 8228-8238. https://doi.org/10.1021/bi00083a025

[18] C. Dargel, F. Gräbitz-Bräuer, R. Geisler, P. Fandrich, Y. Hannappel, L. Porcar, T. Hellweg. Stable DOPG/Glycyrrhizin vesicles with a wide range of mixing ratios: Structure and stability as seen by scattering experiments and Cryo-TEM. *Molecules* 26 (2021) 4959. https://doi.org/10.3390/molecules26164959

[19] A.S. Abreu, B.F.C. Hermenegildo, P.M.T. Ferreira, M.J.R.P. Queiroz, E.M.S. Castanheira. Interaction of fluorescent quinolin-2-one and coumarin derivatives including dipeptides with lipid bilayers. *RSC Advances* 6 (2016) 72141-72148. https://doi.org/10.1039/C6RA14376H

[20] V. Papadopoulou, K. Kosmidis, M. Vlachou, P. Macheras. On the use of the Weibull function for the discernment of drug release mechanisms. *Int. J. Pharm.* 309 (2006) 44–50. https://doi.org/10.1016/j.ijpharm.2005.10.044

[21] X. Hu, B. Yin, K. Cappelle, L. Swevers, G. Smagghe, X. Yang, L. Zhang, Identification of novel agonists and antagonists of the ecdysone receptor by virtual screening. *J. Mol. Graph. Model.* 81 (2018) 77–85. https://doi.org/10.1016/j.jmgm.2018.02.016

[22] T. Harada, Y.Nakagawa, T. Ogura, Y. Yamada, T. Ohe, H. Miyagawa. Virtual screening for ligands of the insect molting hormone receptor. *J. Chem. Inf. Model.* 51 (2011) 296–305. https://doi.org/10.1021/ci100400k

[23] Y. Dong, X. Jiang, T. Liu, Y. Ling, Q. Yang, L. Zhang, X. He. Structure-based virtual screening, compound synthesis, and bioassay for the design of chitinase inhibitors. *J. Agric. Food Chem.* 66 (2018) 3351-3357. https://doi.org/10.1021/acs.jafc.8b00017

[24] J. Liu, M. Liu, Y. Yao, J. Wang, Y. Li, G. Li, Y. Wang. Identification of novel potential β-*N*-Acetyl-D-Hexosaminidase inhibitors by virtual screening, molecular dynamics simulation and MM-PBSA calculations. *Int. J. Mol. Sci.* 13 (2012) 4545–4563. https://doi.org/10.3390/ijms13044545

[25] L. Dong, S. Shen, Y. Xu, L. Wang, Q. Yang, J. Zhang, H. Lu, Identification of novel insect β-*N*-acetylhexosaminidase OfHex1 inhibitors based on virtual screening, biological evaluation, and molecular dynamics simulation. *J. Biomol. Struct. Dyn.* 39 (2021) 1735–1743. https://doi.org/10.1080/07391102.2020.1743758

[26] J. Min, D. Lin, Q. Zhang, J. Zhang, Z. Yu. Structure-based virtual screening of novel inhibitors of the uridyltransferase activity of Xanthomonas oryzae pv. oryzae GlmU. *Eur. J. Med. Chem.* 53 (2012) 150–158. https://doi.org/10.1016/j.ejmech.2012.03.051

[27] R.S. Ramos, J.S. Costa, R.C. Silva, G.V. Costa, A.B.L. Rodrigues, E.M. Rabelo, R.N.P. Souto, C.A. Taft, C.H.T.P. Silva, J.M.C. Rosa, C.B.R. Santos, W.J.C. Macêdo. Identification of potential inhibitors from Pyriproxyfen with insecticidal activity by virtual screening. *Pharmaceuticals* 12 (2019) 20. https://doi.org/10.3390/molecules24162943

[28] C. Riva, P. Suzanne, G. Charpentier, F. Dulin, M.-P. Halm-Lemeille, J. S.-O. Santos. In silico chemical library screening and experimental validation of novel compounds with potential varroacide activities. *Pestic. Biochem. Physiol.* 160 (2019) 11–19. https://doi.org/10.1016/j.pestbp.2019.05.012

[29] Y. Li, , Y. Wang, H. Jiang, J. Deng. Crystal structure of Manduca sexta prophenoloxidase provides insights into the mechanism of type 3 copper enzymes. *Proc. Natl. Acad. Sci.* 106 (2009) 17002–17006. https://doi.org/10.1073/pnas.0906095106

[30] Y. Fu, Y.-X. Liu, T. Kang; Y.-N. Sun, J.-Z. Li, F. Ye. Identification of novel inhibitors of p-hydroxyphenylpyruvate dioxygenase using receptor-based virtual screening. *J. Taiwan Inst. Chem. Eng.* 103 (2019) 33–43. https://doi.org/10.3390/ijms21155546

[31] H. Shen, Z. Li, Y. Jiang, X. Pan, J. Wu, B. Cristofori-Armstrong, J.J. Smith, Y.K.Y. Chin, J. Lei, Q. Zhou, G.F. King, N. Yan. Structural basis for the modulation of voltage-gated sodium channels by animal toxins. *Science* 362 (2018) 1–8. https://doi.org/10.1126/science.aau2596

[32] L.R. Offermann, S.L.Chan, T. Osinski, Y.W. Tan, F.T.Chew, J. Sivaraman, Y.-K. Mok, W. Minor, M. Chruszcz. The major cockroach allergen Bla g 4 binds tyramine and octopamine. *Mol. Immunol.* 60 (2014) 86–94. https://doi.org/10.1016/j.molimm.2014.03.016

[33] J. Cai, X. Du, C.Wang, J. Lin, X. Du. Identification of potential Helicoverpa armigera (Lepidoptera: Noctuidae) sterol carrier protein-2 inhibitors through high-throughput virtual screening. *J. Econ. Entomol.* 110 (2017) 1779–1784. https://doi.org/10.1093/jee/tox157

[34] T. Joshi, T. Joshi, P. Sharma, S. Chandra, V. Pande. Molecular docking and molecular dynamics simulation approach to screen natural compounds for inhibition of Xanthomonas oryzae pv. Oryzae by targeting peptide deformylase. *J. Biomol. Struct. Dyn.* 39 (2021) 823–840. https://doi.org/10.1080/07391102.2020.1719200

[35] G.J. Correy, D. Zaidman, A. Harmelin, S. Carvalho, P.D. Mabbitta, V. Calaora, J. Peter P.J. James, A.C. Kotzeg, C.J. Jackson, N. London. Overcoming insecticide resistance through computational inhibitor design. *Proc. Natl. Acad. Sci.* 116 (2019) 21012–21021. https://doi.org/10.1073/pnas.1909130116

[36] J.D. Laughlin, T.S. Ha, D.N.M. Jones, D.P. Smith. Activation of pheromone-sensitive neurons is mediated by conformational activation of pheromone-binding protein. *Cell* 133 (2008) 1255–1265. https://doi.org/10.1016/j.cell.2008.04.046

[37] P.V. Oliferenko, A.A. Oliferenko, G.I. Poda, Osolodkin, D.I.; G.G. Pillai, U.R. Bernier, M. Tsikolia, M.N. Agramonte, G.G. Clark, K.J. Linthicum, A.R. Katritzky. Promising *aedes aegypti* repellent chemotypes identified through integrated QSAR, virtual ccreening, synthesis, and bioassay. *PLoS One* 8, e64547 (2013). https://doi.org/10.1371/journal.pone.0064547

[38] M. Lill, Computer-aided drug design platform using PyMOL User Guide able of Contents.

[39] G. Jones, P. Willett, R.C. Glen, A.R. Leach, R. Taylor. Development and validation of a genetic algorithm for flexible docking. *J. Mol. Biol.* 267 (1997) 727–748. https://doi.org/10.1006/jmbi.1996.0897

[40] O. Trott, A.J. Olson, AutoDock Vina: Improving the speed and accuracy of docking with a new scoring function, efficient optimization, and multithreading. *J. Comput. Chem.* 31 (2009) 455-461. https://doi.org/10.1002/jcc.21334

[41] T. Sander, J. Freyss, M. von Korff, C. Rufener. DataWarrior: an Open-Source program for chemistry aware data visualization and analysis. *J. Chem. Inf. Model.* 55 (2015) 460–473. https://doi.org/10.1021/ci500588j

[42] N.M. O'Boyle, M. Banck, C.A. James. C. Morley, T. Vandermeersch, G.R. Hutchison. Open Babel: An open chemical toolbox. *J. Cheminform.* 3 (2011) 33. http://www.jcheminf.com/content/3/1/33

[43] A. Waterhouse, M. Bertoni, S. Bienert, G. Studer, G. Tauriello, R. Gumienny, F.T. Heer, de T.A.P. Beer, C. Rempfer, L. Bordoli, R. Lepore, T. Schwede. SWISS-MODEL: Homology modelling of protein structures and complexes. *Nucleic Acids Res.* 46 (2018) W296–W303. 10.1093/nar/gky427

[44] D.A. Case, T.E. Cheatham III, T. Darden, H. Gohlke, R. Luo, K.M. Jr. Merz, A. Onufriev, C. Simmerling, B. Wang, R.J. Woods. The Amber biomolecular simulation programs. *J. Comput. Chem.* 26 (2005) 1668–1688. https://doi.org/10.1002/jcc.20290

[45] J.A. Maier, C. Martinez, K. Kasavajhala, L. Wickstrom, K.E. Hauser, C. Simmerling ff14SB: Improving the accuracy of protein side chain and backbone parameters from ff99SB. *J. Chem. Theory*

Comput. 11 (2015) 3696–3713. https://doi.org/10.1021/acs.jctc.5b00255

[46] J. Wang, R.M. Wolf, J.W. Caldwell, P.A. Kollman, D.A. Case. Development and testing of a General Amber Force Field. *J. Comp. Chem.* 25 (2004) 1157–1174. https://doi.org/10.1002/jcc.20035

[47] M.J. Frisch, G. Trucks, H.B. Schlegel, *et al.* Gaussian 09, Revision A.02. (2016).

[48] D.R. Roe, T. E. Cheatham. PTRAJ and CPPTRAJ: Software for processing and analysis of molecular dynamics trajectory data. *J. Chem. Theory Comput.* 9 (2013) 3084–3095. https://doi.org/10.1021/ct400341p

[49] W. Humphrey, A. Dalke, K. Schulten, VMD: Visual molecular dynamics. *J. Mol. Graph.* 14 (1996) 33–38. https://doi.org/10.1016/0263-7855(96)00018-5

[50] R.P. Magalhães, T.F. Vieira, A. Melo, S.F. Sousa. Identification of novel candidates for inhibition of LasR, a quorum-sensing receptor of multidrug resistant Pseudomonas aeruginosa , through a specialized multi-level in silico approach. *Mol. Syst. Des. Eng.* 7 (2022) 734-446. https://doi.org/10.1039/D2ME00009A

[51] T.F. Vieira, R.P. Magalhães, M. Simões, S.F. Sousa. Drug repurposing targeting pseudomonas aeruginosa MvfR using Dpocking, virtual screening, molecular dynamics, and free - energy calculations. *Antibiotics* 11 (2022) 185. https://doi.org/10.3390/antibiotics11020185

[52] T.F. Vieira, F.G. Martins, J.P. Moreira, T. Barbosa, S.F. Sousa. In *silico* identification of possible inhibitors for Protein Kinase B (PknB) of *Mycobacterium tuberculosis*. *Molecules* 26 (2021) 6162. https://doi.org/10.3390/molecules26206162

[53] F.G. Martins, A. Melo, S.F. Sousa, Identification of new potential inhibitors of quorum sensing through a specialized multi-level computational approach. *Molecules* 26 (2021) 2600. https://doi.org/10.3390/molecules26092600

[54] S. Genheden, U. Ryde. The MM/PBSA and MM/GBSA methods to estimate ligand-binding affinities. *Expert Opin. Drug Discov.* 10 (2015) 449–461. https://doi.org/10.1517/17460441.2015.1032936

[55] C. Jaafar-Maalej, R. Diab, V. Andrieu, A. Elaissari, H. Fessi. Ethanol injection method for hydrophilic and lipophilic drug-loaded liposome preparation. *J. Liposome Res.* 20 (2010) 228–243. https://doi.org/10.3109/08982100903347923

[56] A.A. Noyes, W.R. Whitney. The rate of solution of solid substances in their own solutions. *J. Am. Chem. Soc.* 19 (1987) 930–934. https://doi.org/10.1021/ja02086a003